AIAA SciTech
13-17 January 2014, National Harbor, Maryland
AIAA Atmospheric Flight Mechanics Conference

Asymmetrically Stacked Tori Hypersonic Inflatable Aerodynamic Decelerator Design Study for Mars Entry

Brooke P. Harper[1] and Robert D. Braun[2]
Georgia Institute of Technology, Atlanta, GA, 30332

The Mars missions envisioned in the future require payload mass in excess of the current capable limit for entry vehicle technology. Deployable Hypersonic Inflatable Aerodynamic Decelerators offer one solution to successfully carry out the beginning of an entry architecture as payload mass increases. The majority of the research that has been conducted on these structures only focuses on axisymmetric geometries. In this investigation, aerodynamic performance and stability is examined for three proposed asymmetric families that can generate non-zero lift-to-drag ratios at 0° angle of attack. Advantages of an asymmetric lifting Hypersonic Inflatable Aerodynamic Decelerator include a larger entry corridor, reduced peak heating, larger range, and improved landing accuracy. In particular, there is potential to increase drag performance and reduce ballistic coefficient to mitigate entry, descent, and landing concerns. Blunt, asymmetric Hypersonic Inflatable Aerodynamic Decelerator designs considered are assembled from stacked tori configurations with a base diameter of 20 m and the capability to interface with a 10 m diameter rigid center body. The configurations considered are capable of producing hypersonic lift-to-drag ratios between ~0.6 and ~0.1 for angles of attack ranging from -30° to 20°. A 40 (t) entry mass, approximate mass of large robotic or human scale mission, is assumed resulting in ballistic coefficients from ~78 kg/m^2 to ~113 kg/m^2. From the analyses conducted thus far, encouraging results project asymmetric Hypersonic Inflatable Aerodynamic Decelerators as conceivable candidates for future large scale Mars missions.

Nomenclature

A	=	reference area
α	=	angle of attack
β	=	ballistic coefficient
C_D	=	drag coefficient
C_L	=	lift coefficient
C_p	=	pressure coefficient
CG	=	center of gravity
$C_{m,\alpha}$	=	pitching moment coefficient
L/D	=	lift-to-drag
M	=	Mach number

I. Introduction

ON August 6th, 2012 the world watched as one of the most daunting entry, descent, and landing (EDL) tasks in history was successfully executed with the Mars Science Laboratory (MSL). At 900 kg of payload mass, MSL likely represents the threshold of landed mass possible with Viking-heritage EDL technology that has been a mainstay of Mars landers for decades. [1] The missions envisioned for future Mars robotic and human exploration require significantly larger payload masses. Innovative ideas have to be explored to be able to accomplish prospective endeavors.

Specifically for Mars entry, the atmosphere is too thin to provide substantial deceleration, yet it can generate considerable aerodynamic heating. A sufficiently large amount of drag needs to be produced to decrease vehicle

[1]Graduate Research Assistant, Guggenheim School of Aerospace Engineering, AIAA Student Member
[2]David and Andrew Lewis Associate Professor of Space Technology, Guggenheim School of Aerospace Engineering AIAA Fellow

ballistic coefficient and allow for deceleration high enough in the atmosphere. For traditional rigid aeroshell systems, the maximum aeroshell diameter is limited by the launch vehicle payload fairing. MSL, for example, was limited to 4.5 m.[1] To bypass the payload fairing restriction, larger mass vehicles could use rigid, semi-rigid, or inflatable deployable decelerators (IADs) to reduce their ballistic coefficient.[2]

Proposed and originally flown in the 1960's, IADs assist in the deceleration of an entry vehicle by producing a larger drag area than the entry vehicle's aeroshell alone. If an entry vehicle can obtain a large amount of deceleration in the hypersonic regime, future large robotic and human missions are practical.[1] For this reason, the effort to resurrect IAD research has been strong. In particular, large scale attached Hypersonic Inflatable Aerodynamic Decelerators (HIADs) are one of the principal technologies currently analyzed to achieve these goals.

Programs such as the Inflatable Re-entry Vehicle Experiments (IRVE) have been established to further our knowledge and understanding of HIADs. IRVE II was a technology demonstration mission that confirmed feasibility of using HIADs from the standpoint of inflating the aeroshell exo-atmospherically and maintaining pressure. In addition, it was proven to withstand heating of 2 W/cm^2 necessary for entry survivability. IRVE-3 experienced heating to more than 15 W/cm^2 and demonstrated the effect of lift on a HIAD's trajectory performance.[3] With the accomplishments of IRVE, researchers have seen firsthand the benefits of HIADs and promote their applicability. They are now one possibility to integrate into future missions to Mars. [4]

II. Objective

Current plans for these large missions to Mars call for the landing of 40 - 80 (t).[5] One option for landing large mass payloads at Mars is increasing the entry vehicle's drag area and decreasing its hypersonic ballistic coefficient. A lower ballistic coefficient vehicle decelerates higher in the atmosphere, providing additional timeline and altitude margin necessary for heavier payloads.[6] According to the EDL-SA, some type of IAD implementation is an anticipated necessary component to be able to land larger payloads on the Mars surface.[4]

This investigation assesses the candidacy of three blunt, asymmetric HIAD families proposed for Mars entry by evaluating inherent aerodynamic characteristics for each configuration and making comparisons to a symmetric counterpart.

A. Aerodynamics and Stability

The pressure distribution on the HIADs may be approximated using a Modified Newtonian panel method. A mesh of each HIAD design was generated to calculate the unit inward normal and C_p for each mesh panel. Aerodynamic forces are computed through numerical integration of C_p over the surface of the HIAD body. Performance measures of interest are deduced including *L/D*, C_D, and the hypersonic ballistic coefficient β governed by

$$\beta = \frac{m}{C_D A} \tag{1}$$

where *m* is the entry mass and *A* is the reference area of the HIAD. The magnitude of deceleration and the heating profile associated with the hypersonic regime are strong functions of these parameters.

Equation (1) shows that increasing the drag area will reduce the ballistic coefficient. As such, increasing the diameter of an entry system beyond that allowed by the vehicle fairing would reduce the ballistic coefficient (for a fixed shape). A lower ballistic coefficient will achieve a lower peak heat rate by decelerating at a higher altitude in the Mars atmosphere. This enables a longer entry timeline, larger range, and ability for subsequent entry maneuvers to take place. The aerodynamic characteristics are approximated at M = 24. A 40 (t) entry mass was assumed to attain ballistic coefficient data. The inflatable itself is assumed to add a negligible amount of mass to this type of payload.

Due to the asymmetric nature of the HIADs, there is concern about the stability of each configuration throughout flight in the hypersonic regime. The stability of any entry system is a crucial factor in determining whether a particular design is feasible. Static pitch stability is achieved when $C_{m,\alpha} < 0$. The parameter inherent to a statically stable vehicle is the trim angle, or the angle at which a vehicle returns to after encountering flight disturbances. Understanding the vehicle's trim angle is significant as notably high trim angles promote negative attributes, such as higher heating and wake flow impingement on the payload.

For each HIAD geometry, the approximate angle of attack corresponding to an *L/D* = 0.275 (an average of proposed nominal *L/D* for large payloads)[1,6] is assigned to the trim angle. To determine if the HIAD designs are statically stable, the aerodynamic moments are analyzed about center of gravity (CG) locations that correspond to the respective interpolated trim angles. The allowable CG locations represent where payloads can be effectively

packaged. The array of the CG locations over the body produces a fit CG trim line. Favorable trim lines, ones which allow for flexible payload placement, are anticipated for most HIAD geometries analyzed. If adequate trim lines result, the payload within the entry vehicle may not require complex packaging.

III. HIAD Outer Mold Line Geometry

The aerodynamic and aerothermodynamic performance throughout entry is determined largely by the outer mold line (OML) or exterior shape of the aeroshell. A HIAD would act as a temporary aeroshell forebody that deploys exo-atmospherically from the entry vehicle body. The drag area is increased which helps in dissipating, quickly and efficiently, approximately 90% of the entry vehicle kinetic energy from the point of atmospheric interface. If this can be completed at high altitudes, the difficulty of landing safely is lessened.

Three asymmetric HIAD families are examined and compared to a symmetric HIAD. Overall trends for each type of design are expressed in the analyses to follow.

A. Symmetric HIAD - Baseline

The HIAD geometries proposed are all derivatives of a blunt, 50° sphere-cone with an 8 m nose radius capable of enveloping a maximum aeroshell diameter of 10 m. The base diameter and HIAD height for this particular design is constrained to 20 m and 4 m respectively. Inflatable stacked tori are used to define the structure of each of these HIADs. A rigid nose cap attachment is assumed. The cross section of this structure is represented in Fig. 1.

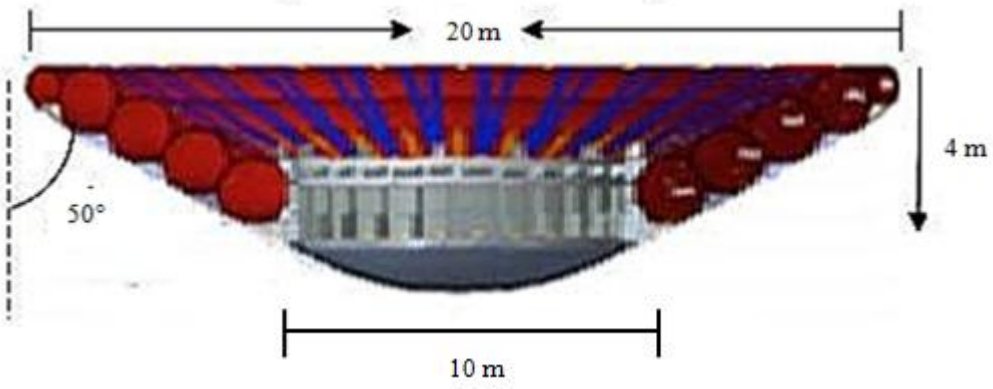

Figure 1. Baseline symmetric HIAD cross section.

To date, all of the landed Mars missions have involved symmetric aeroshell designs. For the following geometries, this baseline design is initially generated and then geometric manipulations occur to produce asymmetric configurations driven by potential advantages of increased *L/D*, ideally with higher C_D, lower ballistic coefficient, smaller trim angles, and reduced heating.

B. Shifted HIAD Family

Shifted HIADs are constructed by defining a shift as a percentage of one-fourth the base diameter. For this design, a 20 m base diameter is retained. When a shift is implemented, the base torus translates through the initial axis of symmetry by the amount of the shift specified, and the intermediate tori follow to maintain geometry. For instance, if a 100% shift is applied, the tori are oriented in a way such that one edge is aligned horizontally. Figure 2 shows the Shifted HIADs that are analyzed in this study.

As a shift is defined, the nose radius must be manipulated in order to maintain smooth connection between the HIAD frustum and nose cap. These adjustments are minor, only slightly changing the overall aeroshell height (from base torus to HIAD nose), while the height of the HIAD (frustum) itself remains unaffected. This trivial variance in the rigid nose cap is deemed negligible.

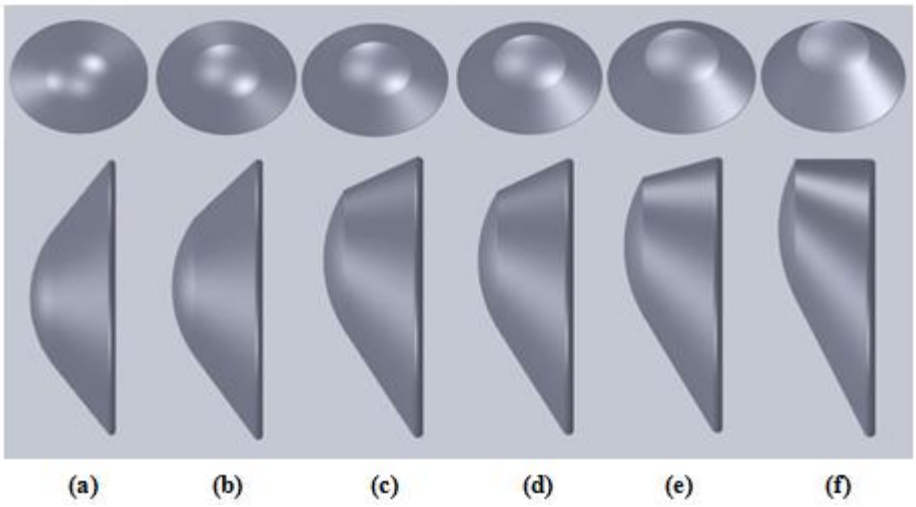

Figure 2. Top and side views of Shifted HIADs at (a) symmetric, (b) 20%, (c) 40%, (d) 60%, (e) 80%, (f) 100%.

C. Flat HIAD Family

A second asymmetric HIAD OML is generated by terminating the tori at a specified length along the 20 m base diameter. All tori larger than the defined length are essentially cut to produce a flat top. The result of this process is displayed in Fig. 3 with Small, Medium, and Large Cut Flat HIADs. The lengths chosen to yield these designs were $18\frac{1}{3}$ m, $16\frac{2}{3}$ m, and 15 m respectively.

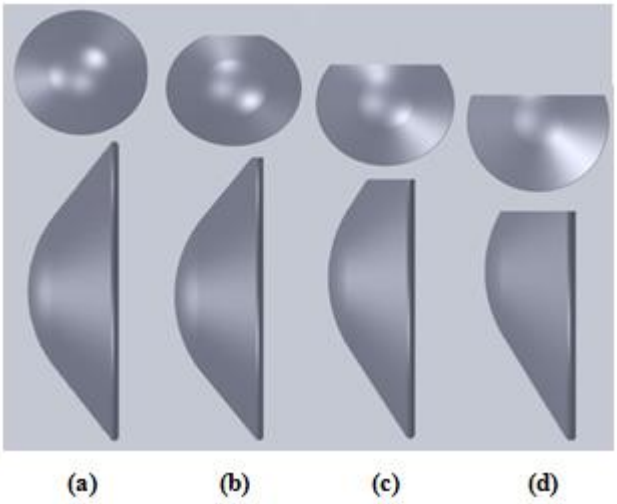

Figure 3. Top and side views of Flat HIADs for (a) symmetric, (b) Small Cut, (c) Medium Cut, (d) Large Cut.

It is hypothesized that these HIADs may possess favorable aerothermodynamic consideration upon entry. However, by this method, the reference area is reduced in comparison to the symmetric HIAD. While the drag area is less with each cut, it is possible that the resulting *L/D* and ballistic coefficients do not deviate considerably from the symmetric baseline. If this is the case, the anticipated aerothermodynamic benefit may outweigh the slight aerodynamic variances. It is important to note that the manufacturability of these asymmetric components raises the complexity of such a design.

D. Biconic HIAD Family

Biconic HIADs are produced by slicing through the top of an original symmetric HIAD at specified angles. The cases examined in this study are 30°, 20°, and 10° planar cuts along the top of the HIAD to produce biconic shapes seen in Fig. 4.

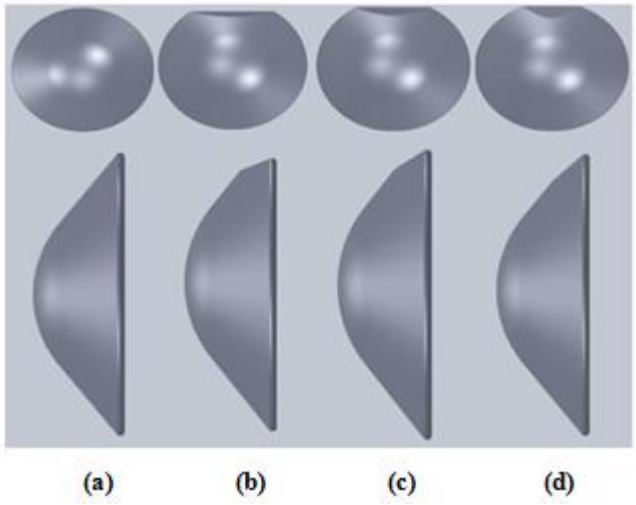

Figure 4. Top and side views of Biconic HIADs at (a) symmetric, (b) 30°, (c) 20°, (d) 10°.

These slices are made at the midpoint height of the HIAD frustum. The maximum allowable biconic configuration is a 50° (cone angle) planar cut which would actually resemble a Flat HIAD OML. Like the assumptions made for the Flat HIAD configuration, the objective is to maintain respectable aerodynamic performance but gain improved aerothermal response.

IV. Results

A. Hypersonic Aerodynamic Force Coefficients

Primary focus is on the *L/D* and ballistic coefficients for these asymmetric blunt body HIADs are illustrated in Figs. 5-10. The hypersonic aerodynamic force coefficients for each type of HIAD have been determined by Modified Newtonian flow theory and are compared to its symmetric counterpart. Attaining improved *L/D* performance coupled with reduced ballistic coefficients for the asymmetric HIADs is ideal. The angle of attack range is chosen to be -30° to 20°.

1. Shifted HIADs

Represented in Fig. 5, *L/D* performance is improved in comparison to the symmetric HIAD for each Shifted HIAD configuration over this range of angle of attack, α. The augmentation of the C_L coefficients is clearly depicted with the maximum *L/D* performance obtained for a 100% shift. At α between -30° and -15° high C_L and lower C_D values are the contributors to higher *L/D* capability. However, as angle of attack decreases (i.e. becomes less negative), the C_D for all Shifted HIADs exceeds the baseline. In fact, all Shifted HIAD cases analyzed surpass the symmetric HIAD C_D by α = -10°.

This trade off between *L/D* and C_D becomes more apparent when β is examined as shown in Fig. 6. Again, while higher angles of attack enhance *L/D*, C_D values are less than that of the symmetric HIAD and ultimately result in higher ballistic coefficients. When the C_D betters the symmetric HIAD capability at lower angles of attack, β is consequently reduced in conjunction with greater *L/D*. The results captured in the dashed box from *L/D* = 0 - 0.4 exhibit where every Shifted HIAD case promotes ideal aerodynamic features.

For *L/D* = 0.275 (that proposed for high mass Mars entries), Shifted HIADs meet the goal of increasing *L/D* performance by amplifying both C_L and C_D while decreasing β. Furthermore, because this occurs at lower angles of attack, the trim angles necessary for stability will be lessened. A stability analysis investigating the effects of these trim angles follows. From an aerodynamic standpoint, Shifted HIADs are feasible candidates for Mars entry.

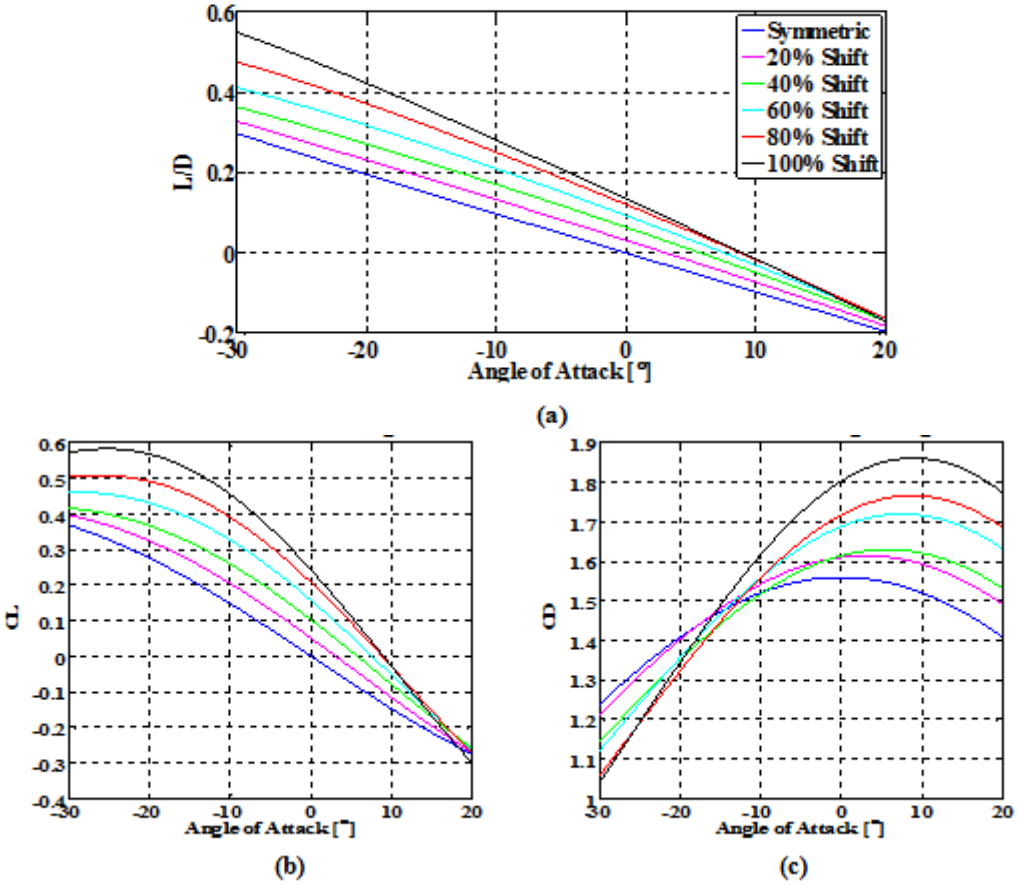

Figure 5. Aerodynamic data for Shifted HIADs (a) L/D, (b) C_L, and (c) C_D vs. angle of attack.

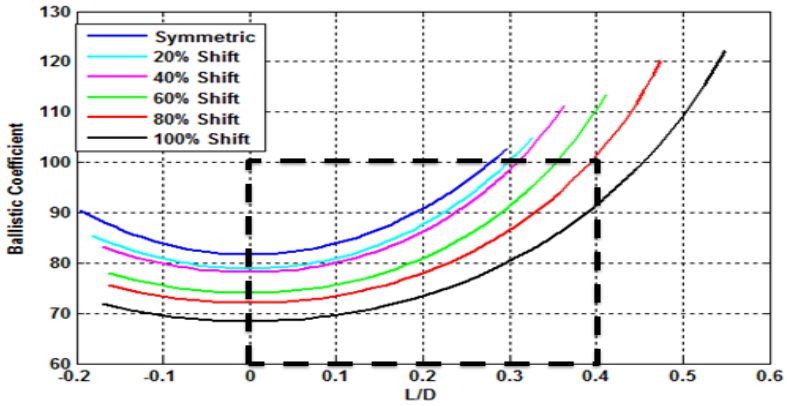

Figure 6. Ballistic Coefficient vs. L/D for Shifted HIADs.

2. Flat HIADs

As anticipated, aerodynamic results for Flat HIADs are dominated by their reduction in reference area. However, it should be noted that *L/D* is improved by an increased C_L and decreased C_D values over all angles of attack shown in Fig. 7. The greatest attainable *L/D* for these configurations is 0.375 at -30° angle of attack. If the Mars EDL architecture requires a higher *L/D*, these HIADs would meet those needs.

In addition, as shown in Fig. 8, the rise in β is not drastic. Even for the Large Cut Flat HIAD where C_D is significantly smaller than that of the symmetric HIAD, variation in β is not large. However, β becomes a concern if $L/D > 0.3$ is a requirement.

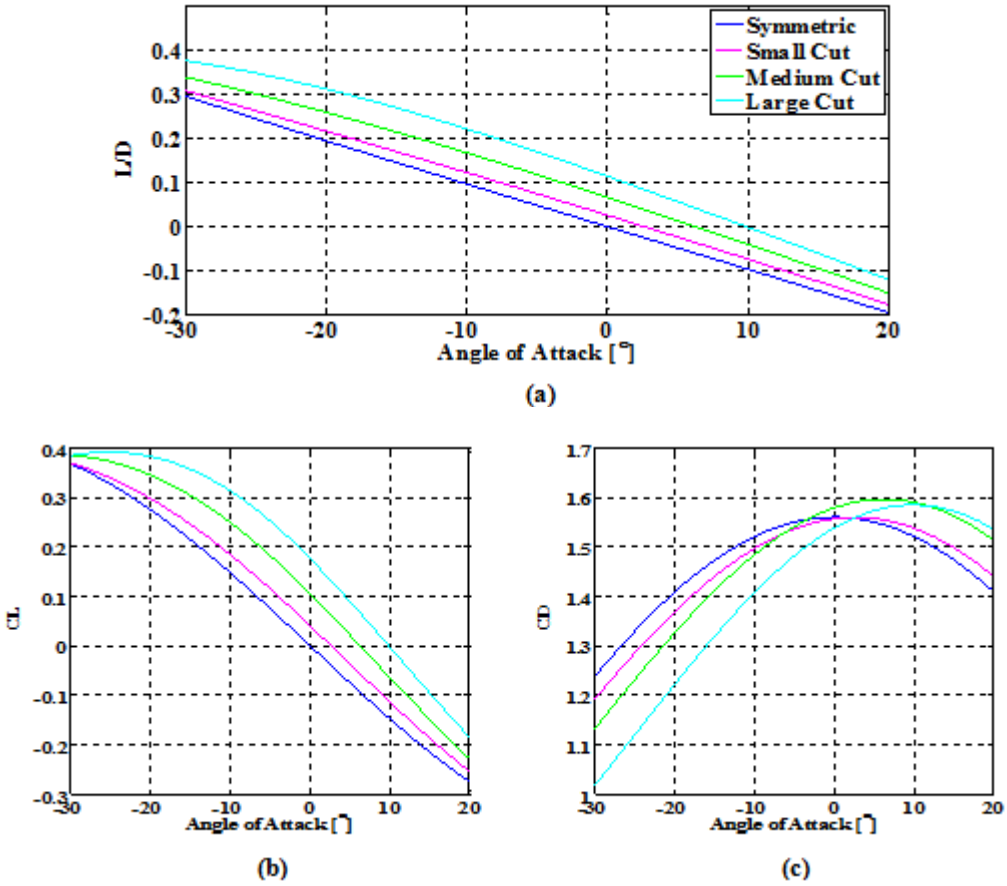

Figure 7. Aerodynamic data for Flat HIADs (a) L/D, (b) C_L, and (c) C_D vs. angle of attack.

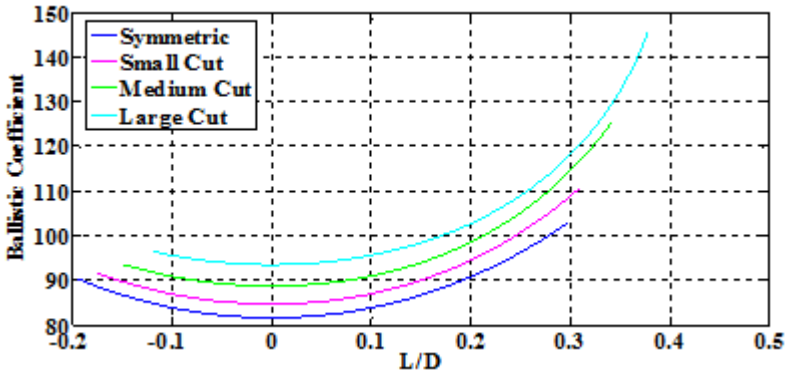

Figure 8. Ballistic Coefficient vs. L/D for Flat HIADs.

These configurations may not be aerodynamically superior to Shifted HIADs but may be able to compensate for these losses by showing favorable stability for sufficient packaging and the ability to withstand the harsh aerothermal loads expected in any entry sequence.

3. Biconic HIADs

The aerodynamic response for Biconic HIADs is analogous to the Flat HIADs. The slight loss in reference area does not strengthen any aerodynamic properties of interest. In fact, as shown in Figs. 9 and 10, there is not much gained at all from this type of design manipulation. The *L/D* captured is nearly identical to the symmetric HIAD and

β is increased for each case. This is not to say the Biconic HIADs are an overall weak choice, they just do not exemplify overall better aerodynamic performance.

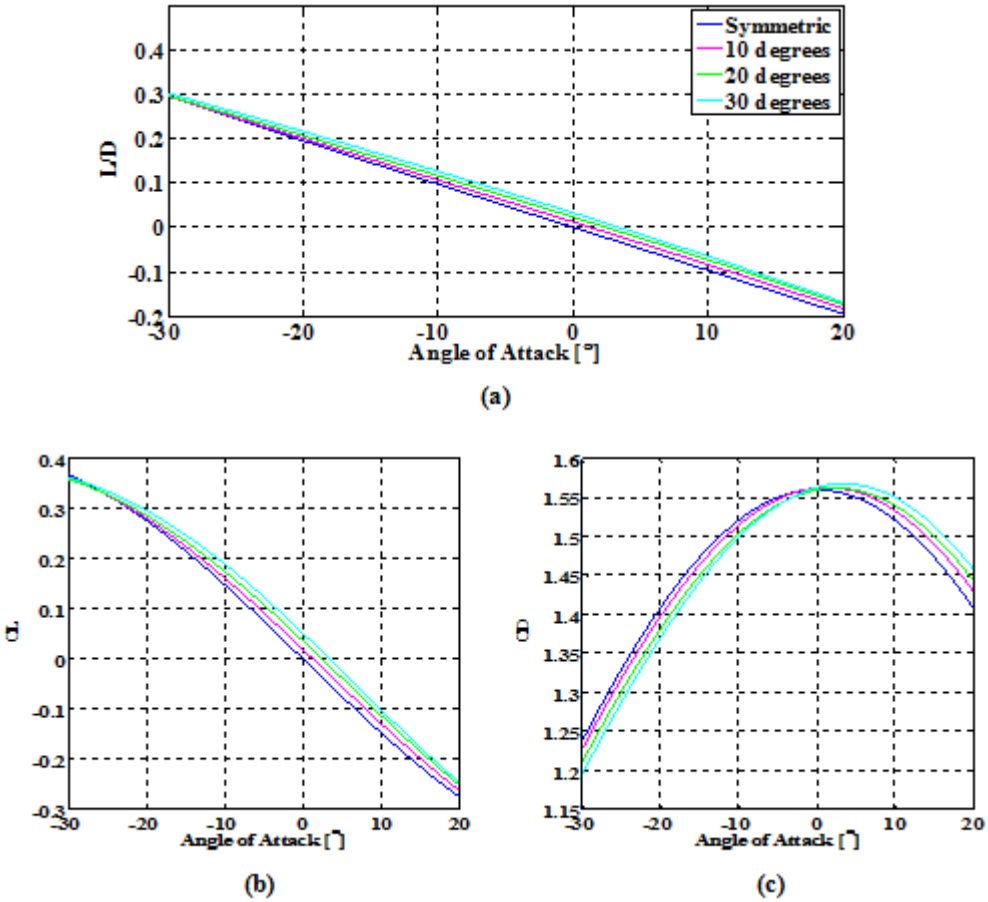

Figure 9. Aerodynamic data for Biconic HIADs (a) L/D, (b) C_L, and (c) C_D vs. angle of attack.

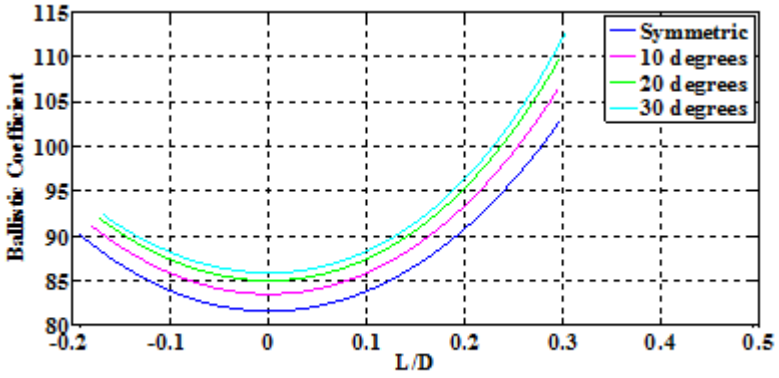

Figure 10. Ballistic Coefficient vs. L/D for Biconic HIADs

4. Force Coefficient Summary

In general, for all HIAD types analyzed, *L/D* performance may be enhanced. However, for the majority of the HIAD cases investigated it is attributed to a rise in C_L and lower C_D when compared to the symmetric HIAD.

Fortunately, there was encouraging data retrieved from some of the Shifted HIAD cases where an increase in *L/D* and decrease in β is obtained.

B. Hypersonic Pitch Stability

A stability analysis was also conducted under the assumption that the entry architecture targets a nominal *L/D* = 0.275. For each asymmetric HIAD design, the angle of attack corresponding to that *L/D* was interpolated and set as the trim angle. Table 1 shows each respective trim angle, C_D, and β for all configurations.

Table 1. Trim angles, C_D, and β at *L/D* = 0.275 for each HIAD geometry

Configuration	Trim Angle (at *L/D* = 0.275)	Drag Coefficient	Ballistic Coefficient (kg/m^2)
Symmetric	-27.9	1.2785	99.59
20% Shift	-24.6	1.3201	96.45
40% Shift	-20.4	1.3436	94.76
60% Shift	-16	1.4451	88.1
80% Shift	-12	1.5165	83.96
100% Shift	-9.6	1.6265	78.28
Flat Small Cut	-26.24	1.2632	104.56
Flat Medium Cut	-21.75	1.2941	109.46
Flat Large Cut	-15.51	1.3096	113.13
Biconic 10°	-27.9	1.2663	103.07
Biconic 20°	-27.6	1.2546	105.86
Biconic 30°	-26.8	1.255	107.27

Figure 11 shows the correlation between β and trim angle of attack for the asymmetric HIADs investigated. For the Shifted HIAD cases, the lower trim angles are associated with greater C_D values compared to the symmetric HIAD. These results are supported by Fig. 5. As the Flat HIAD and Biconic HIAD do not demonstrate this overall trend, excluding the 10° Biconic, the trim angles are all smaller than the symmetric counterpart which is a very beneficial attribute. Reduced aerothermal and lateral aerodynamic loads are anticipated on the leeside of the HIADs as trim angles are reduced.

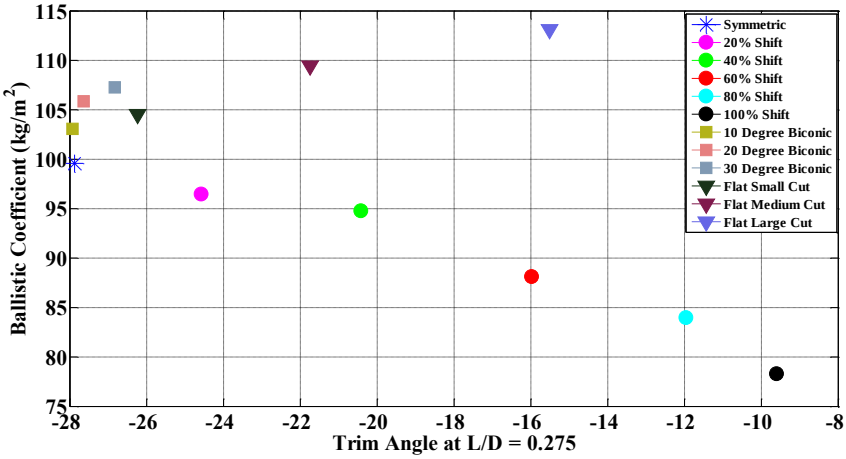

Figure 11. Ballistic coefficients for each HIAD geometry at trim angles capable of L/D = 0.275.

The location of the CG is a significant factor in determining how the payload can be effectively packaged. For most blunt body shapes as the CG moves towards the aft of the vehicle stability is difficult to attain. Thus, an exploration to establish possible CG locations corresponding with each HIADs trim angle at L/D = 0.275 was

carried out. Each CG trim line is shown over the body of all HIAD cases in Fig. 12. The aerodynamic moments at the CG locations along the trim lines validate these trim positions by concluding $C_{m,\alpha} = 0$.

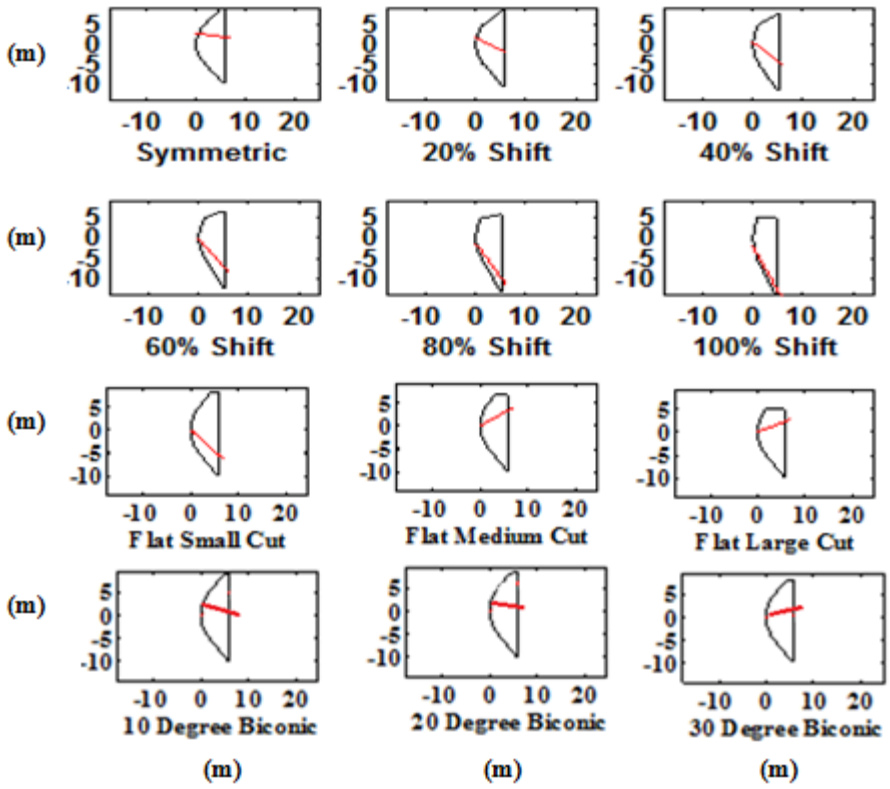

Figure 12. Center of gravity trim lines capable of trim angles of attack where L/D = 0.275.

While static stability is ensured for these cases, special caution must be placed on selecting a viable CG location for a payload. For trim lines that exhibit steeper slopes (i.e. 60-100% Shifted HIAD), efficient packaging is more difficult as the available CG locations are placed near the frustum boundaries of the HIAD narrowing the amount of space available for the payload. For these cases, assuming a 10 m rigid center body, portions of the CG trim lines become extraneous as they extend beyond the center body geometries.

The best configurations for payload placement is seen for the Biconic HIADs in which the trim line nearly extends horizontally from the nose of the vehicle. Assuming a symmetric payload, the CG can be placed along this axis. However, it should be noted that once the HIAD is jettisoned, new aerodynamic moments will be produced which will likely change the stability of an entry vehicle. Other measures will likely need to be taken to ensure static stability through the full EDL sequence.

V. Conclusions

The analyses presented in this paper give a glimpse into the potential for asymmetric HIADs. The tradeoff between ballistic coefficient and *L/D* performance is illustrated. When compared to its symmetric counterpart, for a large range of angle of attack, Shifted HIADs present encouraging results with the ability to improve *L/D* performance by increasing both lift and drag. As a result, ballistic coefficient is reduced. For the other asymmetric HIADs analyzed in this study, *L/D* was always improved; however it was due to the increase in C_L only. For the Flat and Biconic OMLs, the change in area was the prevailing asymmetric factor resulting in decreased C_D values and higher ballistic coefficients. However, for nearly all asymmetric HIAD geometries, the trim angle of attack at *L/D* = 0.275 is lower which has beneficial attributes. Slightly higher ballistic coefficients may be considered acceptable in exchange for lower trim angles and/or aerothermodynamic advantages. Furthermore, all asymmetric HIAD configurations were shown to be statically stable during hypersonic flight. Trim lines justify an array of

potential CG locations for each type of configuration. Overall, the aerodynamic performance and or stability benefits intrinsic to asymmetric HIADs may promote their use in future high mass Mars landing missions.

References

[1] Braun, R., Manning, R., "Mars Exploration Entry, Descent, and Landing Challenges," *Journal of Spacecraft and Rockets*, Vol. 44, No. 2, March-April 2007, p. 310-323.

[2] Adler, M. et al, "Draft Entry, Descent, and Landing Roadmap: Technology Area 09," NASA, November 2010.

[3] Litton, D. et al, "Inflatable Re-entry Vehicle Experiment (IRVE) – 4 Overview"

[4] Dwyer-Cianciolo, Alicia M., et al. "Entry, Descent and Landing Systems Analysis Study: Phase 1 Report." (2010).

[5] Wells, G. et al, "Entry, Descent, and Landing Challenges of Human Mars Exploration," *29th Annual AAS Guidance and Control Conference*, Breckenridge, Colorado, February 2008.

[6] Lafleur, Jarret M., "Angle of Attack Modulation for Mars Entry Terminal State Optimization,"*AIAA Atmospheric Flight Mechanics Conference, Chicago*, Illinois, August 2009.